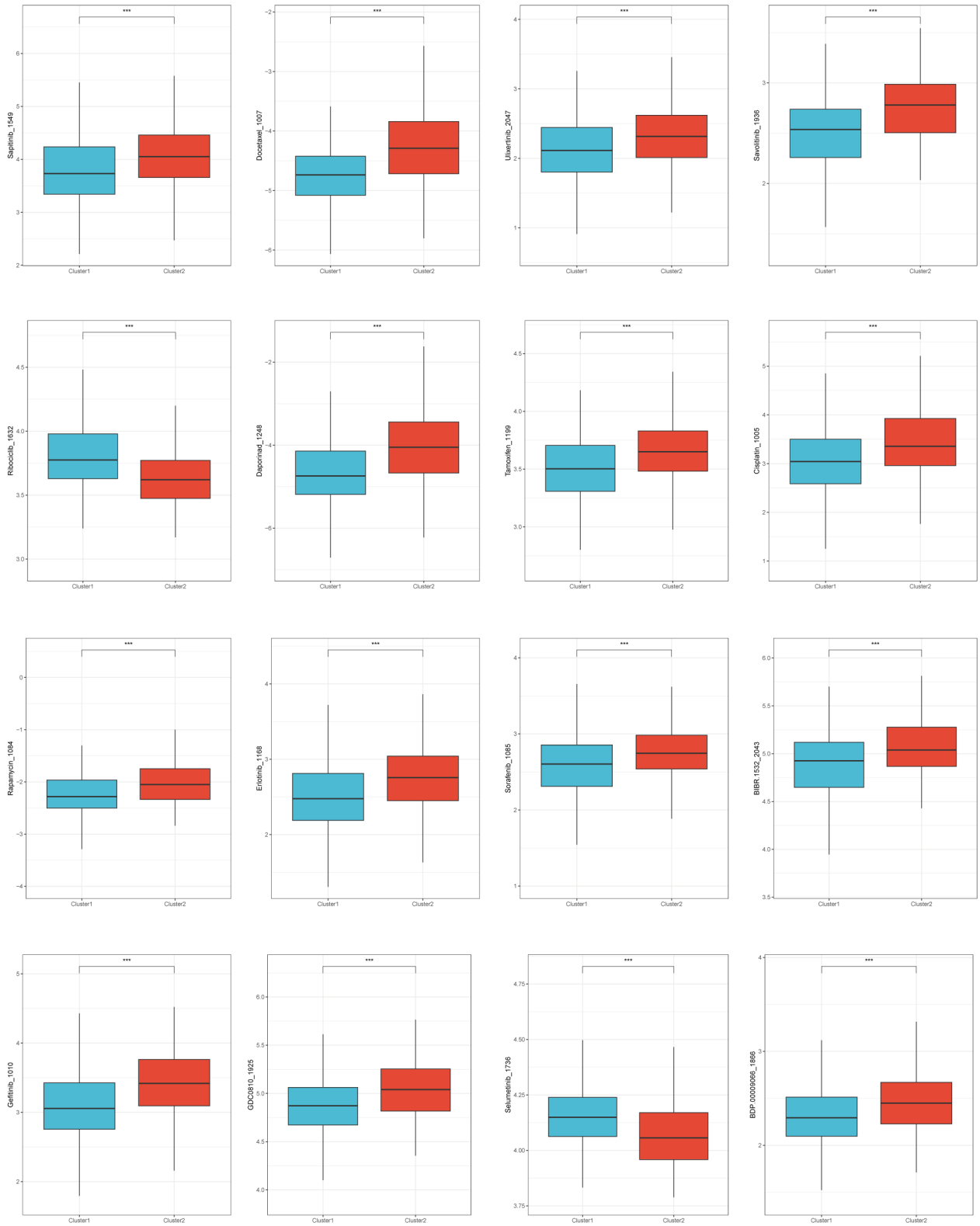

Figure S1 Drug sensitivity prediction. Violin plots comparing the predicted half-maximal inhibitory concentration (IC50) of anti-cancer drugs from the GDSC database between Cluster1 and Cluster2. ***P<0.001 by Wilcoxon rank-sum test.

https://dx.doi.org/10.21037/tcr-2026-1-0302

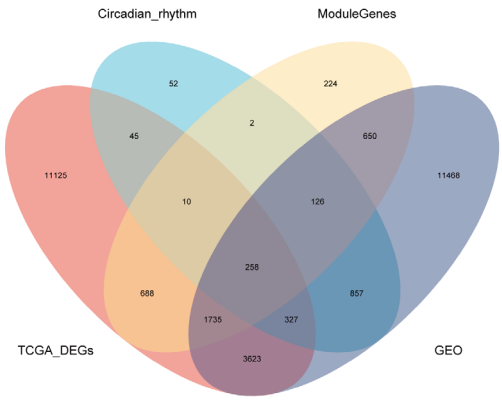

Figure S2 Four-way Venn diagram of gene sets used for differentially expressed candidate genes identification. Overlap among (i) TCGA-LUSC DEGs, (ii) circadian-rhythm genes from CGDB, (iii) WGCNA module genes, and (iv) GEO sequenced genes. Numbers indicate unique gene counts within each intersection; percentages are omitted for clarity. The 258 genes shared by all four sets were taken forward as candidate genes for downstream analyses.

Table S1 StepCox[both] + GBM model Relative Influence

var	rel.inf
TREM1	23.1076
CLDN5	17.8719
NKX2.1	15.5566
ALPL	15.364
CLDN1	14.4136
FGG	13.6863

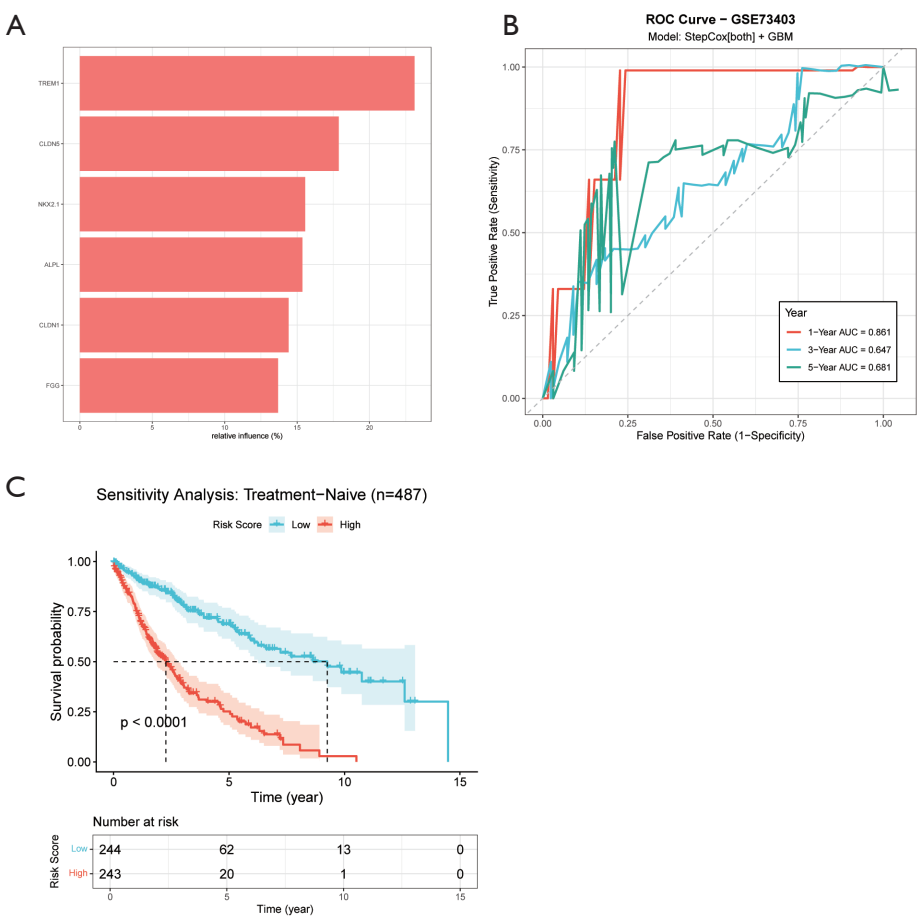

Figure S3 CIGPS based prognostic model. (A) Relative Influence of the component genes derived from the final Ran StepCox+ GBM model. Horizontal bars indicate Relative Influence. (B) Time-dependent receiver operating characteristic (ROC) curves predicting 1-, 3-, and 5-year overall survival in the validation cohort. (C)Sensitivity analysis excluding patients with prior systemic therapy. Kaplan–Meier survival curves comparing overall survival between high-risk and low-risk groups in the treatment-naïve cohort (n = 487). The prognostic discrimination remained virtually unchanged compared with the full cohort (C-index: 0.716 *vs.* 0.717). Log-rank P < 0.0001. The number-at-risk table is shown below the plot.

https://dx.doi.org/10.21037/tcr-2026-1-0302

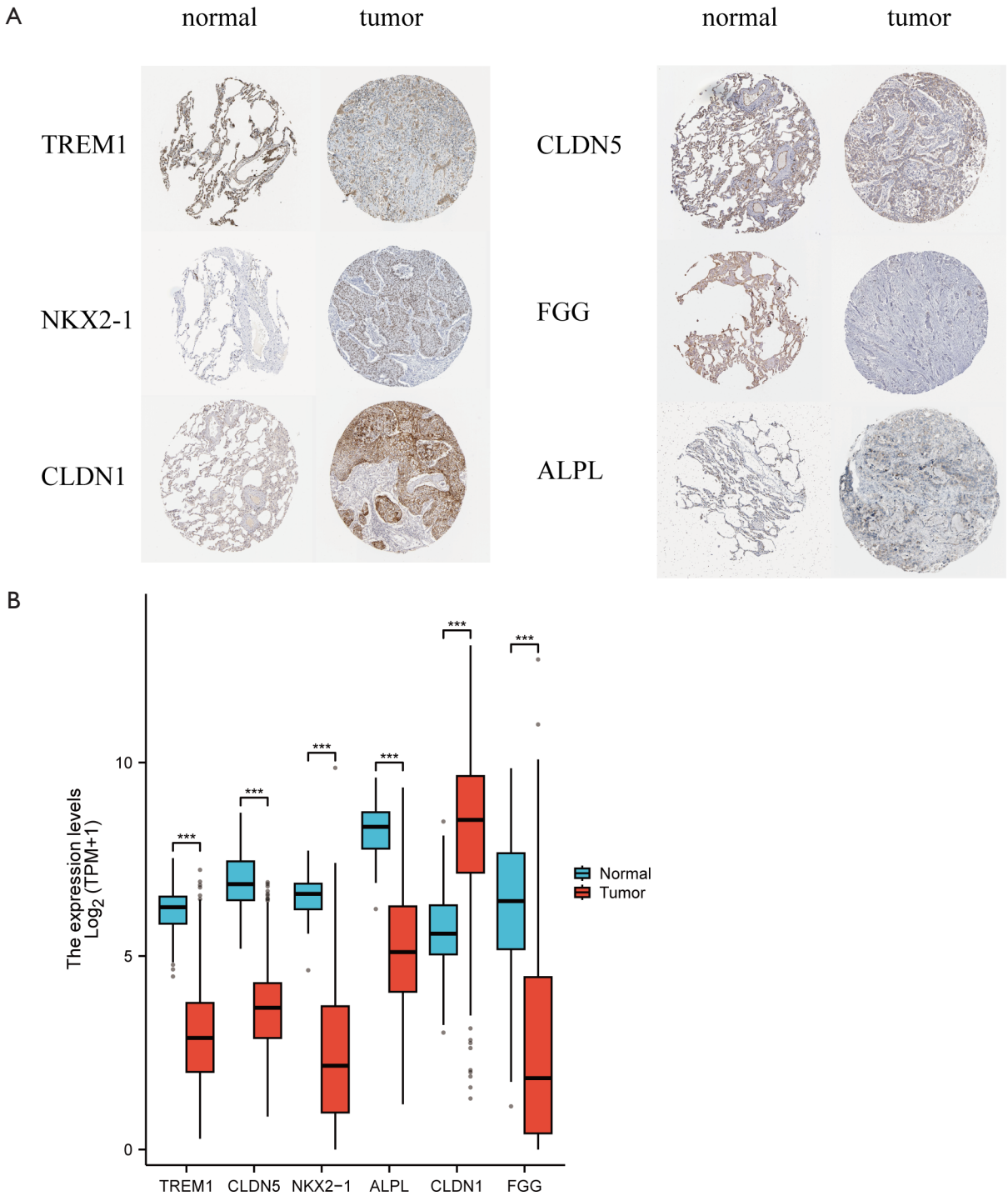

Figure S4 CIGPS expression. (A) CIGPS expression in normal and lung adenocarcinoma tissues obtained by HPA. (B)Boxplot showing the expression levels of CIGPS genes between the normal and tumor tissue in TCGA-LUSC.

https://dx.doi.org/10.21037/tcr-2026-1-0302

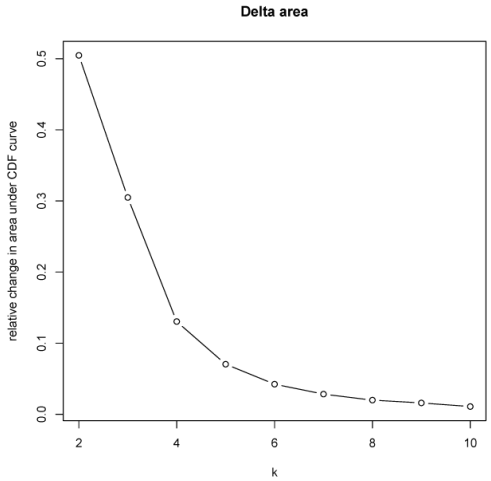

Figure S5 Molecular subtyping based on the 6-gene CIGPS. (A) cumulative distribution function (CDF) plots and Delta area.

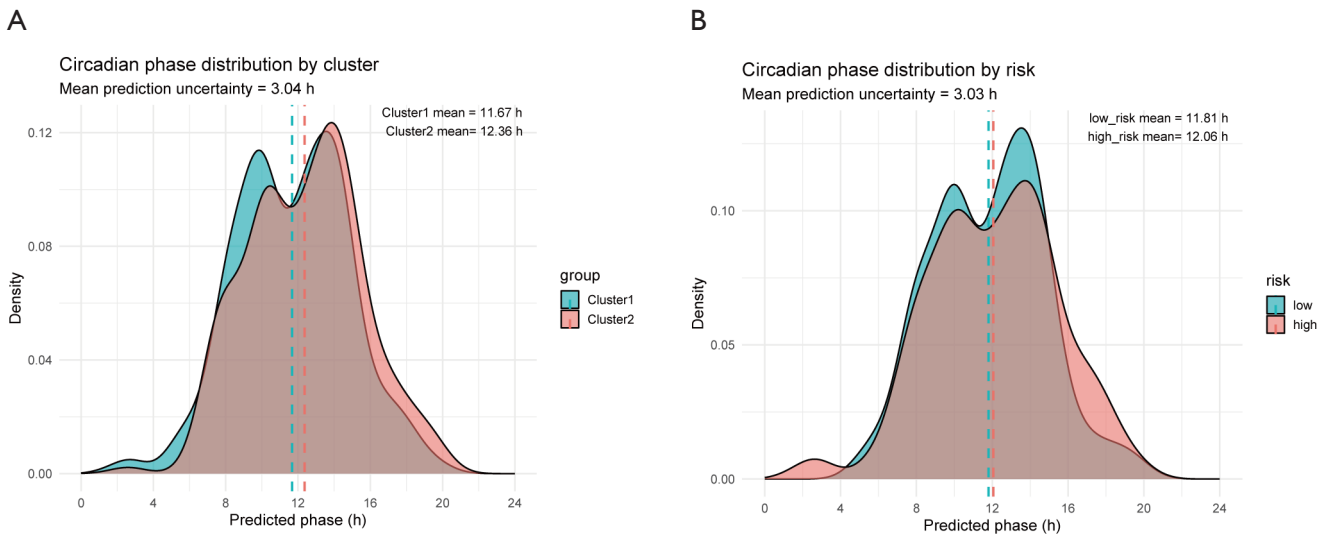

Figure S6 Circadian rhythm analysis in TCGA-LUSC. (A,B) Circadian phase density of TCGA-LUSC samples predicted by TimeTeller. Dashed lines indicate the mean phase of each cluster.

https://dx.doi.org/10.21037/tcr-2026-1-0302

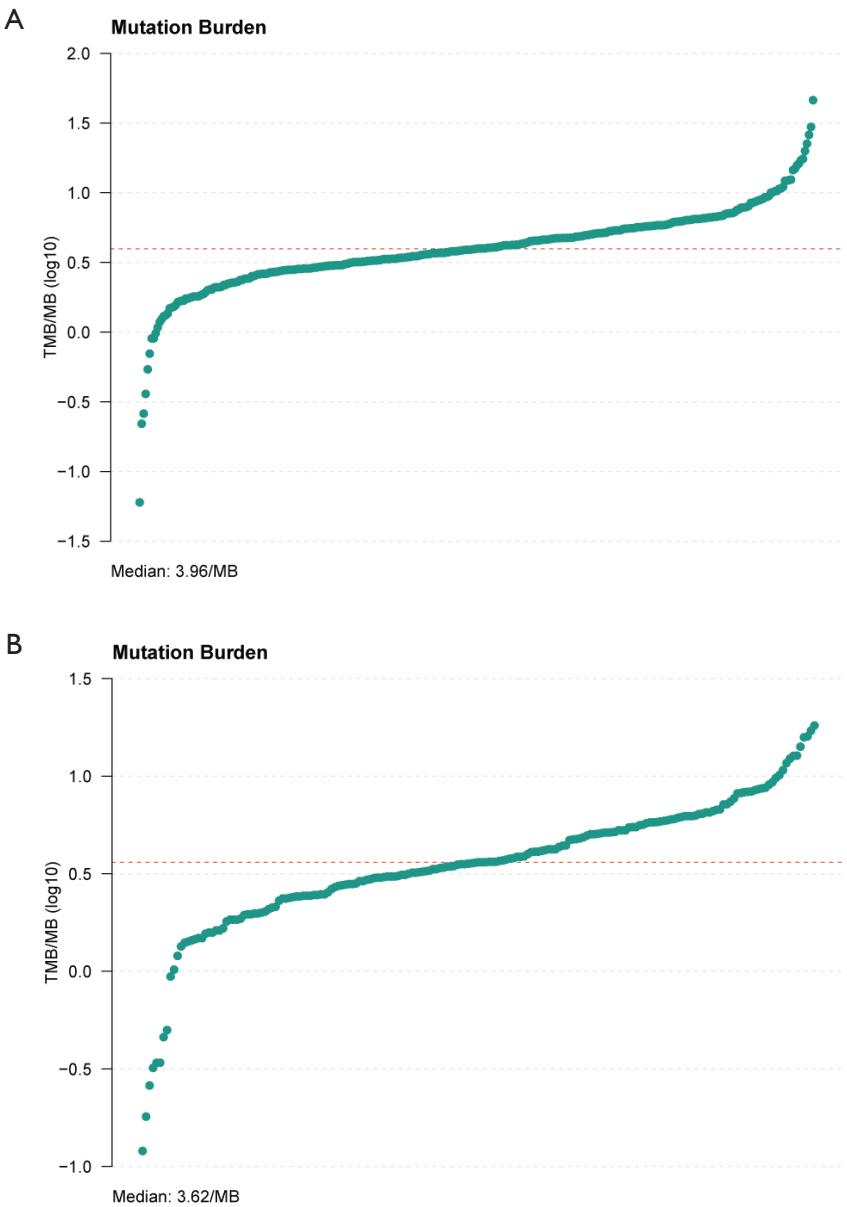

Figure S7 tumor mutation analysis. (A,B) tumor mutation burden (TMB) between Cluster1 (A) and Cluster2 (B).

https://dx.doi.org/10.21037/tcr-2026-1-0302

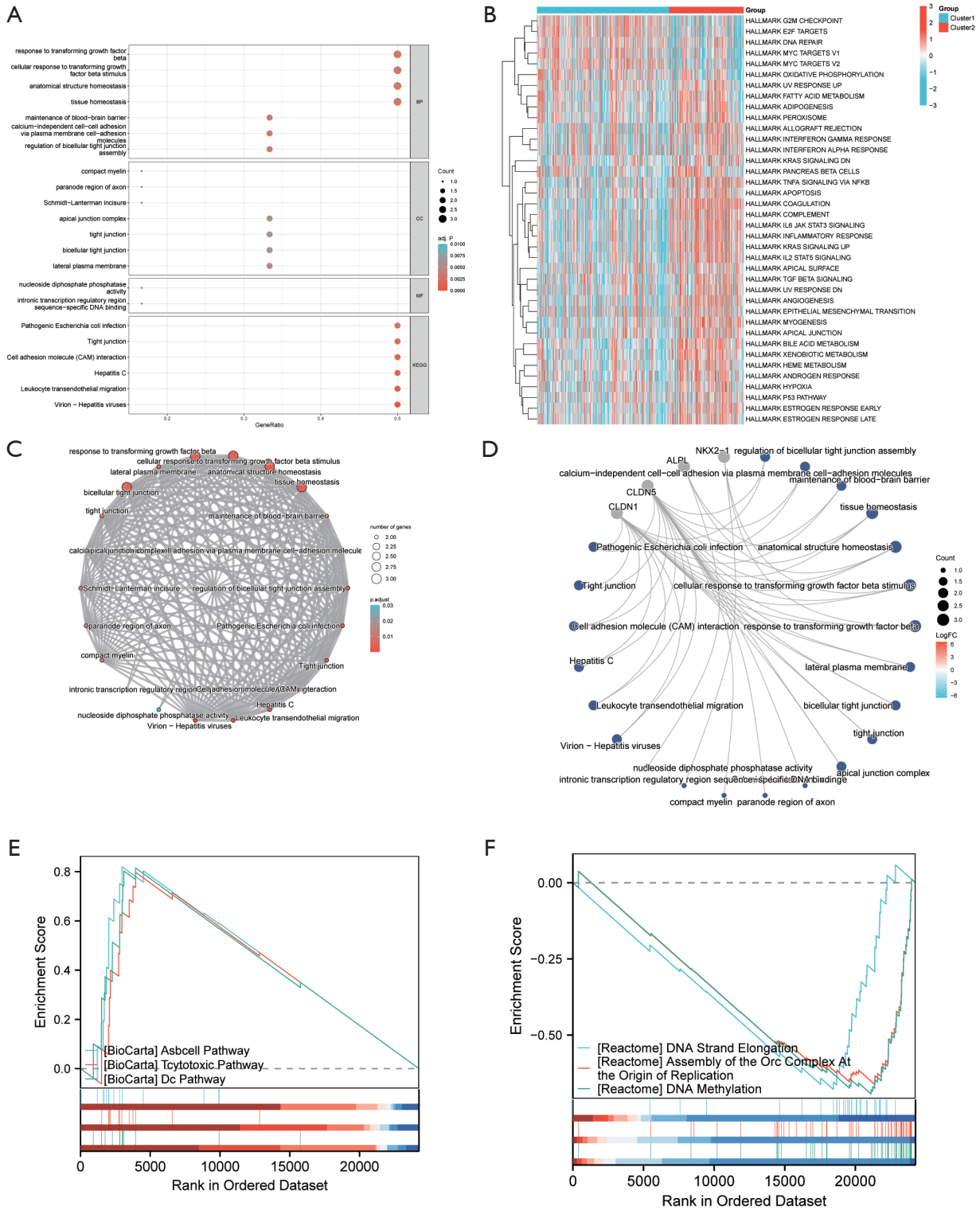

Figure S8 Functional enrichment analysis of the CIGPS. (A) Bar plot showing the significantly enriched Gene Ontology (GO) terms and KEGG pathways. (B) Heatmap of enrichment scores from Gene Set Variation Analysis (GSVA) using Hallmark gene sets in TCGA-LUSC subtypes. (C) Enrichment map (emap) and (D) network plot visualizing relationships among enriched GO terms and KEGG pathways. (E, F) Gene Set Enrichment Analysis (GSEA) results for Cluster1 versus Cluster2. Terms with P<0.05 and FDR q-value <0.25 were considered significant.

https://dx.doi.org/10.21037/tcr-2026-1-0302

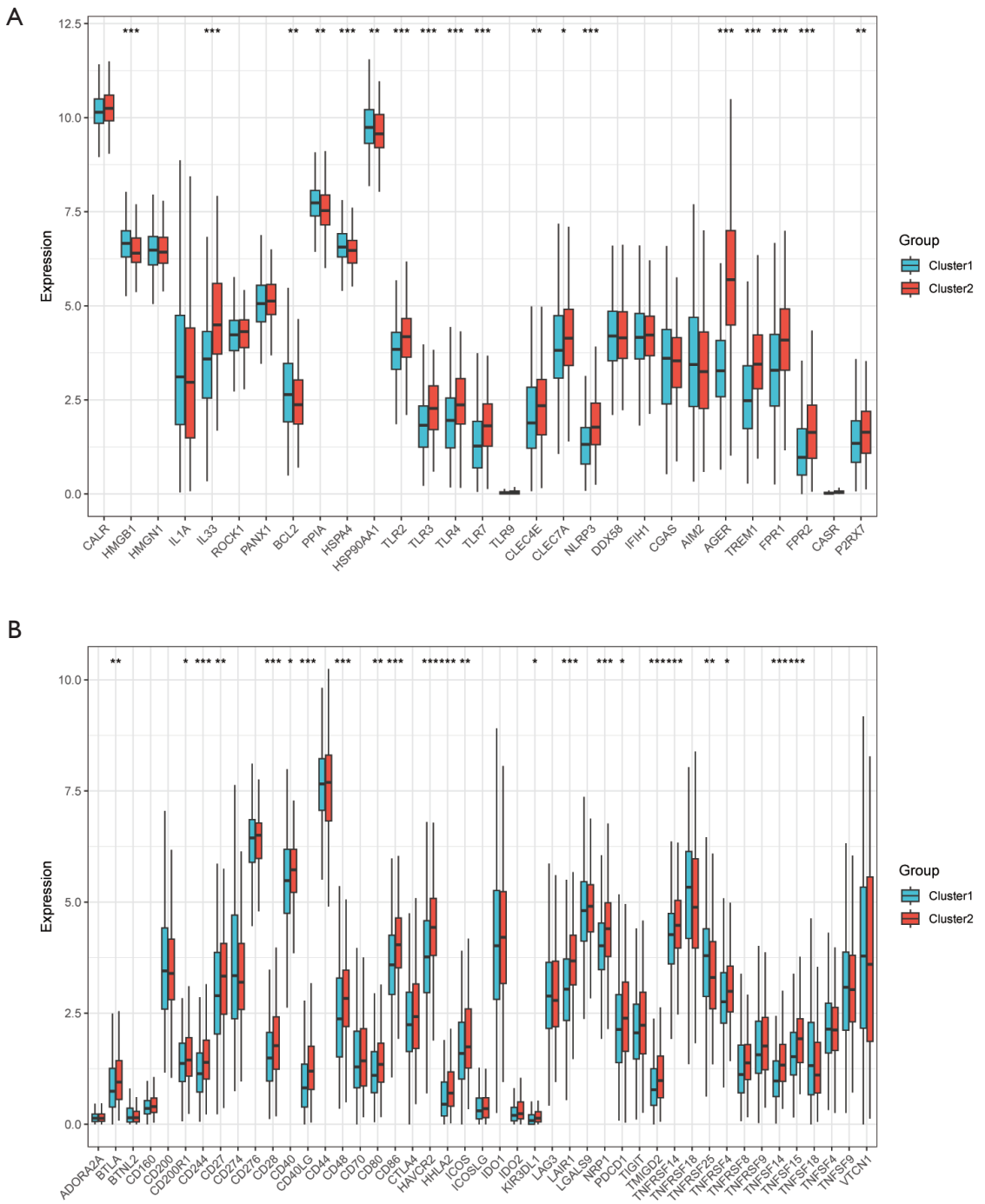

Figure S9 Immunotherapy-related analyses. (A,B) Expression differences of immune-related gene sets between the two consensus-cluster subgroups of LUSC. (A) ICD genes (Immunogenic Cell Death). (B) ICG genes (Immune Checkpoint Genes).

https://dx.doi.org/10.21037/tcr-2026-1-0302

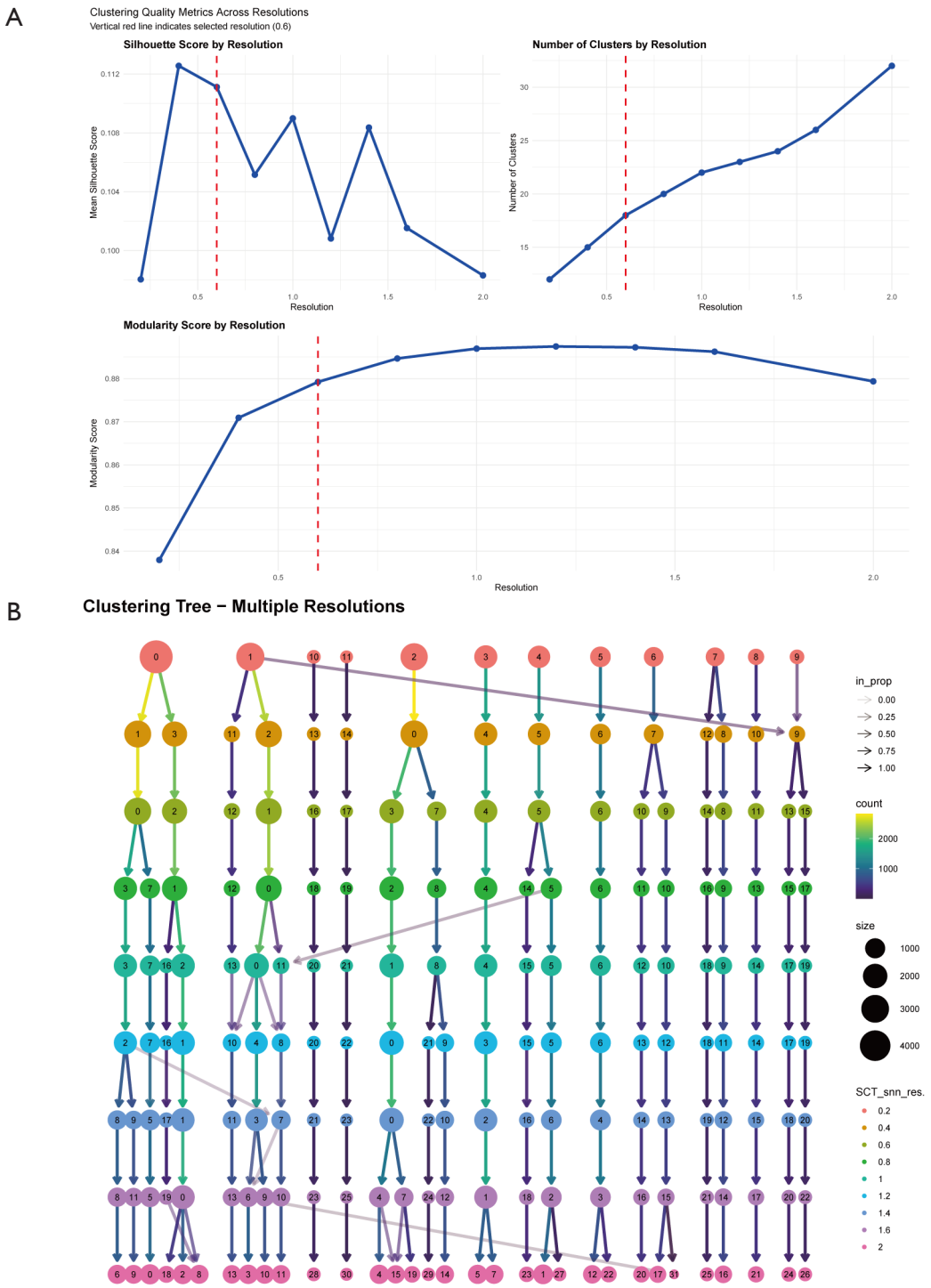

Figure S10 Comprehensive resolution parameter optimization for single-cell clustering. (A) Quantitative assessment of clustering quality across nine resolution parameters (0.2, 0.4, 0.6, 0.8, 1.0, 1.2, 1.4, 1.6, 2.0). (B) Clustree analysis visualizing cluster stability and relationships across resolutions.

https://dx.doi.org/10.21037/tcr-2026-1-0302